Rock Engineering and Rock Mechanics: Structures in and on Rock Masses – Alejano, Perucho, Olalla & Jiménez (Eds)
© 2014 Taylor & Francis Group, London, 978-1-138-00149-7

Temperature-confining pressure coupling effects on the permeability of three rock types under triaxial compression

A.K.M.B. Alam, Y. Fujii & D. Fukuda
Rock Mechanics Laboratory, Sustainable Resources Engineering, Hokkaido University, Sapporo, Japan

M. Niioka
Mitsubishi Corporation Exploration, Tokyo, Japan

ABSTRACT: Triaxial compression tests were carried out at 295K and 353K under confining pressure of 1–15 MPa for Shikotsu welded tuff, Kimachi sandstone and Inada granite. The samples were kept for 24 hr consolidation and then axial compression was applied measuring permeability. Permeability decreased monotonously for Shikotsu welded tuff. The permeability decreased first, began to increase before peak load and showed almost constant value in the residual strength state for Kimachi sandstone and Inada granite. Permeability decreased by failure for Shikotsu welded tuff. It increased due to failure under low confining pressures but decreased under high confining pressures for Kimachi sandstone. It increased due to failure for Inada granite. The permeability at 353K was lower than that at 295K for all of the three types of rock. The mechanisms of the permeability decrease are also shown.

1 INTRODUCTION

Stress redistribution and change in permeability happen within the Excavation disturbed Zone (EdZ) and Excavation Damaged Zone (EDZ). This puts significant impacts on short- as well as long-term stability of excavations as Hydro Mechanical (HM) processes. The EDZ can be under low or relatively high confining pressure (Fig. 1) and temperature change in rock mass which significantly affects the sealability and permeability of radioactive waste repositories (Hudson et al. 2005, Rutqvist et al. 2005) can be introduced either by human activities or by natural processes. The objective of this research is to know the influences of temperature-confining pressure coupling on permeability as Thermo Hydro Mechanical (THM) processes.

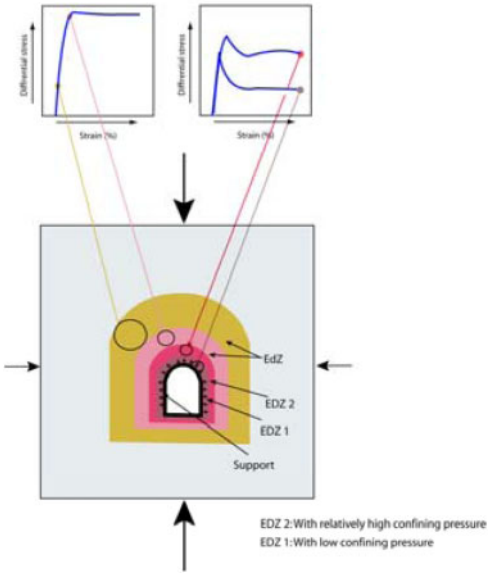

Figure 1. EdZ and EDZ around an underground excavation.

2 MATERIALS AND METHODS

Three rock types were considered for the experiments. (i) Shikotsu welded tuff: highest effective porosity of 37% with low UCSS (saturated uniaxial compressive strength) of 14 MPa. (ii) Kimchi sandstone: 19% effective porosity with UCSS of 21 MPa. (iii) Inada granite: low effective porosity of 0.6% with UCSS of 181 MPa.

The ultra compact triaxial cell (Fig. 2, Alam et al. 2014) which was covered with a heater to maintain target temperature (295K and 353K) was used for the experiments. The lower attachment was connected to the syringe pump. The upper attachment was opened to the atmosphere in constant flow method or attached to a reservoir for transient pulse method to measure permeability.

24 hours consolidation was carried out under target consolidation pressure and temperature for each specimen. Afterward, constant strain rate compression at 10^{-5} s^{-1} (0.036 mm/min) was applied on the consolidated samples. The compression was continued until the stroke based axial strain reached at 10% for Shikotsu welded tuff measuring permeability by

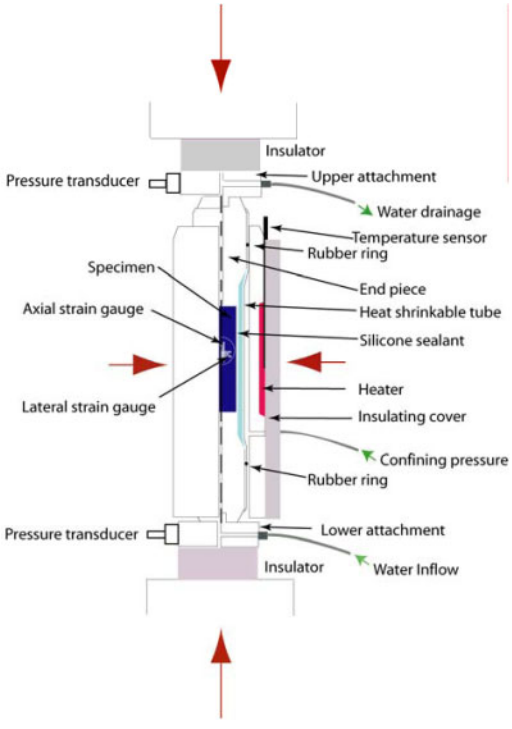

Figure 2. Ultra compact triaxial cell with heater. Showing water inflow and water drainage during constant flow method.

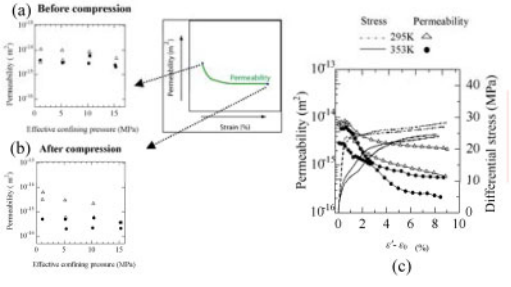

Figure 3. Permeability of Shikotsu welded tuff.

constant flow method or 7% for Kimachi sandstone and Inada granite measuring permeability by transient pulse method. Data sampling interval was 10 s.

3 RESULTS AND DISCUSSION

3.1 Shikotsu welded tuff

After 24 hours of consolidation, the permeability at 295K was higher than the permeability at 353K (Fig. 3a) and permeability under 15 MPa confining pressure (P_c) was the lowest. Permeability decreased monotonously during compression (Fig. 3c). The post compression permeability at 295K decreased with confining pressure (Fig. 3b). On the other hand, it was

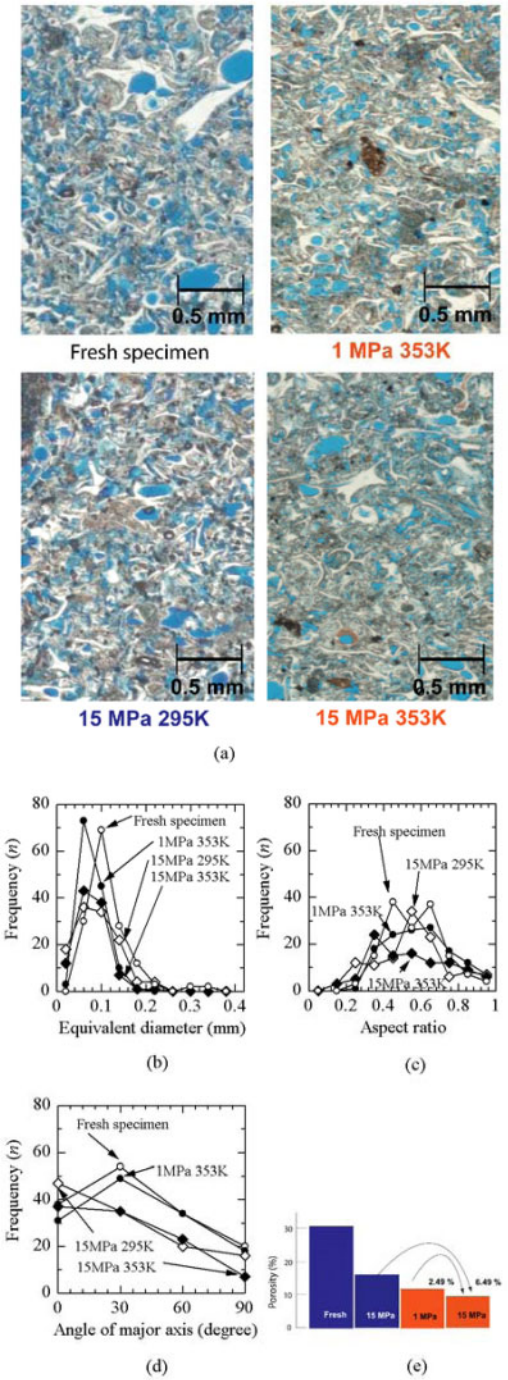

Figure 4. Thin section image and analyses of consolidated specimens of Shikotsu welded tuff.

almost independent of confining pressure at 353K and as low as that under 15 MPa P_c at 295K.

In the thin section image analyses of 24 hours consolidated specimen (Fig. 4a), the porosity decreased by 2.49% from 1 MPa to 15 MPa P_c at 353K and

6.49% from 295K to 353K under 15 MPa P_c (Fig. 4e). 0.10 mm equivalent diameter pores were dominant for fresh specimen whereas 0.06 mm equivalent diameter pores were dominant at 353K. Significant decrease of 0.14 mm from 295K to 353K under 15 MPa P_c (Fig. 4b) was observed. The frequency of pores having aspect ratio of 0.45–0.65 which was dominant under 1 MPa P_c at 353K decreased under 15 MPa P_c (Fig. 4c). Pores parallel to the horizontal flow layer still dominated at 15 MPa P_c (Fig. 4d).

In CT images of post compression specimens, main rupture plane with sub rupture planes and several fractures were formed under 1 MPa P_c at 295K (Fig. 5a). On the other hand, only one main rupture plane occurred at 353K (Fig. 5b). The porosity at 353K in the thin section analyses was 10.0% less in the region far from the rupture plane than that at 295K (Fig. 5k). The rupture planes were absent in 15 MPa P_c cases and the porosity at 353K was lower than that at 295K by 4.63% (Fig. 5k).

Under 1 MPa P_c, far from the rupture plane, 0.14 mm and 0.10 mm equivalent diameter pores significantly decreased and 0.06 mm increased at 353K (Fig. 5e). Under 15 MPa P_c, significant decrease of 0.10 mm pores and increase of 0.06 mm pores were observed at 353K (Fig. 5f). The frequency of aspect ratio 0.25 to 0.65 decreased at 353K under 1 MPa P_c and 0.35 increased under 15 MPa P_c at 353K (Fig. 5h). Pores parallel to the horizontal flow layer were dominant (Fig. 5i, j).

From the observations, it is obvious that pore collapse (Zamman et al. 1994) occurred during axial compression even under low confining pressures (Figs. 5 and 6) causing the permeability decrease. The highest permeability decrease under 15 MPa P_c at 295K was easily achieved even under 1 MPa P_c at 353K (Fig. 5b) because of low porosity matrix due to enhanced pore collapse by thermal activation.

3.2 *Kimachi sandstone*

After 24 hours of consolidation, the permeability at 353K under >5 MPa P_c was slightly lower than that at 295K (Fig. 7a). During compression, permeability decreased first, began to increase before peak load, showed almost stable value at residual strength state (Fig. 7d). The minimum permeability decreased with confining pressure and no significant difference was observed between 295K and 353K (Fig. 7b). The post compression permeability decreased with confining pressure and the permeability at 353K was slightly lower than that at 295K (Fig. 7c).

For the specimens after 24 hours consolidation (Fig. 8a), the thickness of cementing materials decreased both by either confining pressure or temperature (Fig. 8b). The thickness at 353K was smaller even under 1 MPa P_c than that under 15 MPa P_c at 295K.

In the post compression specimens, main and sub-rupture planes with several fractures were observed in the CT images under 1 MPa P_c at 295K (Fig. 9a).

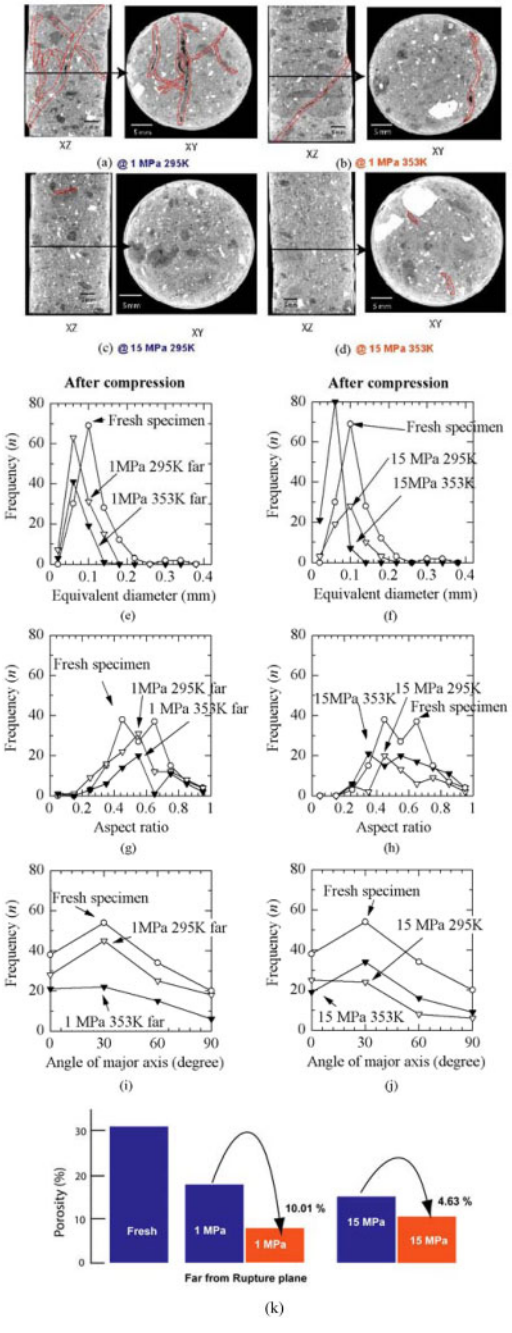

Figure 5. CT images and thin section image analyses of post compression specimens of Shikotsu welded tuff.

Only one main rupture plane with sub rupture plane was observed at 353K (Fig. 9b). The average thickness of cementing material (Fig. 9g) for the specimen was 0.20 mm under 1 MPa P_c at 295K and 0.19 mm at 353K of the thin section images (Fig. 9h). There were two rupture planes under 3 MPa P_c at 295K (Fig. 9c) but only one in the case of 353K (Fig. 9d). The rupture planes were absent in the cases of 15 MPa P_c

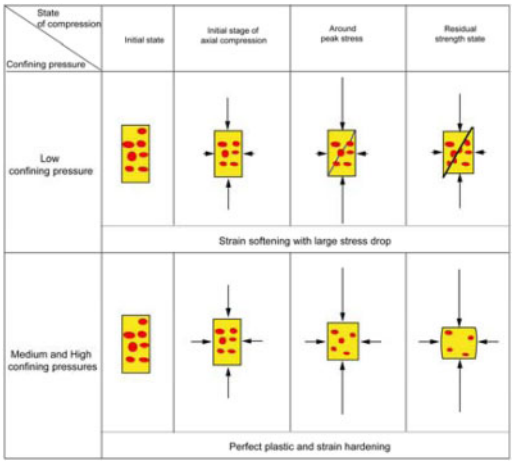

Figure 6. Confining pressure effects on structural changes of Shikotsu welded tuff.

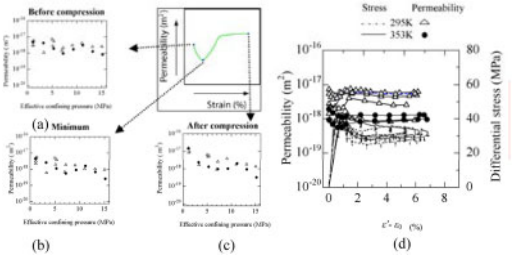

Figure 7. Permeability of Kimachi sandstone.

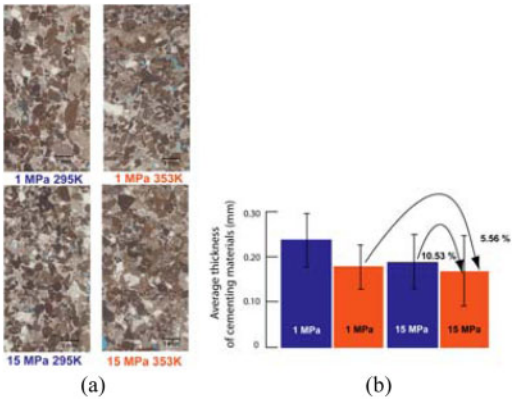

Figure 8. Thin section images and thickness of cementing materials of consolidated specimens of Kimachi sandstone.

(Fig. 9e, f). The average thickness of cementing material under 15 MPa P_c (Fig. 9g) was 0.15 mm at 295K and 0.14 mm at 353K (Fig. 9h).

From the observations, it can be considered that the decrease of permeability at consolidation and initial stage of axial compression was due to elastic as well as plastic closure of inclined microcracks (Alam et al. 2014) and its increase was due to nucleation and

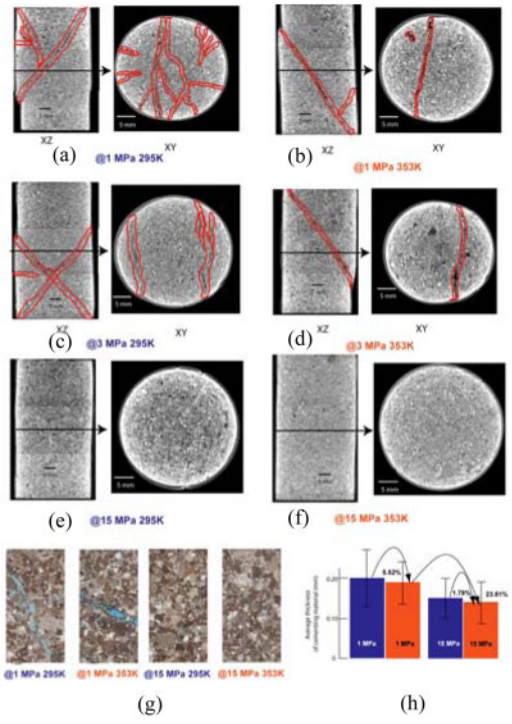

Figure 9. CT and thin section images and thickness of cementing materials of post compression specimens of Kimachi sandstone.

coalescence of microcracks (Kranz 1983) (Fig. 10). The decrease in number of rupture planes in the post compression specimens with confining pressures (Fig. 9, 10) was due to large plastic deformation of cementing materials. The post compression permeability at 353K was slightly lower than that at 295K (Fig. 7c) because of enhancement of the plastic deformation by thermal activation.

3.3 *Inada granite*

After 24 hour consolidation, the permeability at 353K was lower than that at 295K (Fig. 11a). Permeability decreased, began to increase before peak load again and showed almost stable value under residual strength state during compression (Fig. 11d). The minimum permeability at 353K was slightly lower than that at 295K and the difference was larger in low confining pressures (Fig. 11b). The post compression permeability decreased with confining pressure up to 9 MPa P_c at 295K or 7 MPa P_c at 353K, and increased afterward (Fig. 11c). Permeability at 353K was significantly lower than that at 295K.

The decrease of permeability by consolidation with confining pressure was mainly due to elastic closure of inclined microcracks. This was not observed in the images as they were prepared after unloading. In the post compression specimen, under 1 MPa P_c at 295K, there occurred one distinct thick main rupture plane with many sub rupture planes and fractures in CT

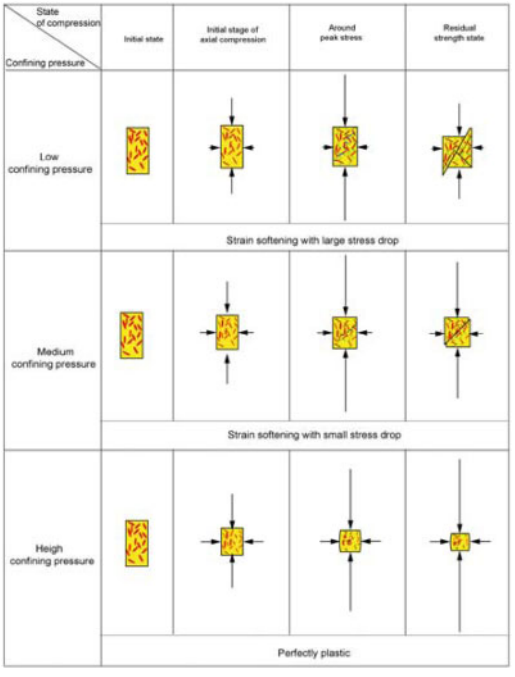

Figure 10. Confining pressure effect on structural changes of Kimachi sandstone.

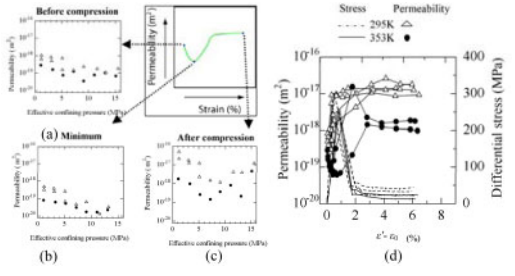

Figure 11. Permeability of Inada granite.

images (Fig. 12a). The rupture plane was the network of microcracks and there were axial cracks from biotite (Fig. 12c). Under 7 MPa P_c at 295K, one main thin rupture plane was observed without the axial cracks from biotite (Fig. 12f). Two main rupture planes formed at 295K under 15 MPa P_c (Fig. 12h). One main thin rupture plane with subrupture plane (Fig. 12b, g) as well as elongation of biotite along the rupture plane (Fig. 12d, e) was observed for 1 MPa and 7 MPa P_c at 353K. Many subrupture planes and fractures formed under 15 MPa at 353K (Fig. 12i).

Several rupture planes and fractures caused the high permeability at 295K under low confining pressures with axial cracks from biotite; Single rupture plane and absence of axial cracks from biotite caused the low permeability for medium confining pressure; Multi rupture planes caused the high permeability under high confining pressure (Fig. 12, 13). The post compression permeability at 353K was lower than that at

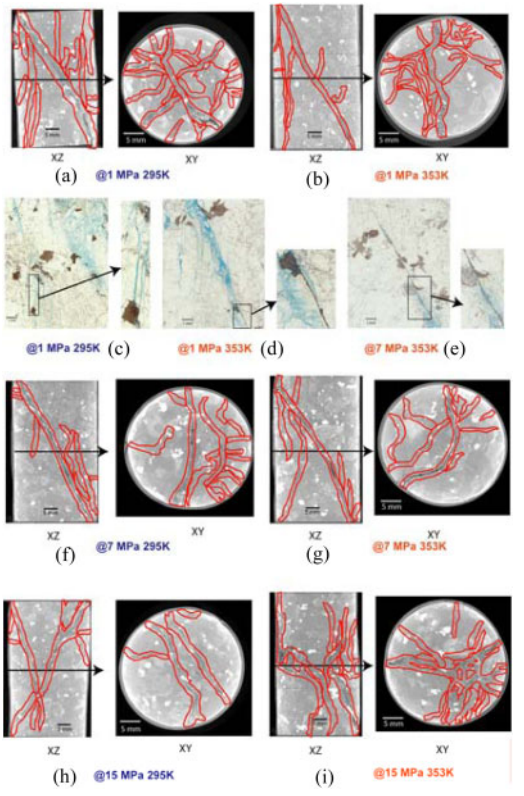

Figure 12. CT and thin section images of post compression specimens of Inada granite.

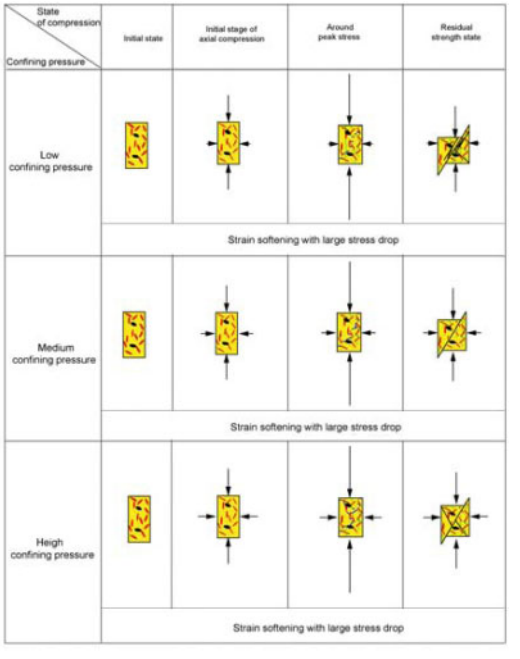

Figure 13. Confining pressure effect on structural changes of Inada granite.

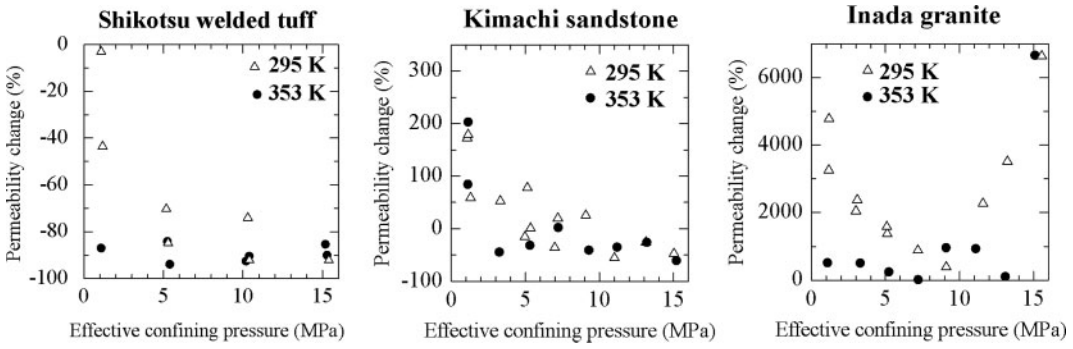

Figure 14. Permeability change due to failure.

295K (Fig. 11c) because of decrease in thickness of the main rupture plane, decrease of subrupture planes, fractures and the microcracks from biotite grains due to enhancement of viscous deformation of mineral grains by thermal activation (Fig. 13). The elongation of biotite along the rupture plane (Fig. 12d, e) was possibly another reason of the low permeability. The multi rupture planes under high confining pressures were caused by high stress concentration between the stiff rupture planes.

4 PERMEABILITY CHANGE (Fig. 14)

For Shikotsu welded tuff, the permeability decreased from consolidation to post compression by failure. The decreased ratio became larger with confining pressure from 2% to 92% at 295K. On the other hand, the ratio was from 84% to 94% and almost independent of confining pressure at 353K.

For Kimachi sandstone, the permeability at 295K increased by as high as 180% by failure under low confining pressures. It however decreased by as low as 47% under high confining pressures. The permeability at 353K decreased by almost the same amount as that under 15 MPa P_c at 295K except for 1 MPa P_c.

For Inada granite at 295K, the permeability increased as high as 4780% by failure under 1 MPa P_c. The increase amount decreased until 9 MPa P_c to 394% and increased again up to 6640% at 15 MPa P_c. At 353K, the permeability increase was as low as that under 9 MPa P_c at 295K and did not showed confining pressure dependency except for the result under 15 MPa P_c.

5 CONCLUSIONS

Permeability of three types of rock under triaxial compression was measured at 295K and 353K. The main findings are as follows.

(i) Permeability decreased monotonously for Shikotsu welded tuff. The permeability decreased first, began to increase before peak load and showed almost constant value in the residual strength state for Kimachi sandstone and Inada granite.

(ii) Permeability decreased by failure for Shikotsu welded tuff. It increased due to failure under low confining pressures but decreased under high confining pressures for Kimachi sandstone. It increased due to failure for Inada granite.

(iii) The permeability at 353K was lower than that at 295K for all of the three types of rock. The main mechanisms of the decrease were enhancement of pore collapse for Shikotsu welded tuff, plastic deformation of cementing materials for Kimachi sandstone and viscous deformation of mineral grains for Inada granite. Thermal activation acted for all of these mechanisms.

ACKNOWLEDGEMENT

This work was partly supported by KAKENHI (22560804). We are grateful to Professor Katsuhiko Kaneko (Laboratory of Terrestrial Engineering, Hokkaido University), for his kind help with the micro-focus X-ray CT scanner.

REFERENCES

Alam, A.K.M.B., Niioka, M., Fujii, Y., Fukuda, D. & Kodama J. 2014 (In press). Effect of confining pressure on the permeability of three rock types under compression. *Int J of Rock Mech Min Sci.*

Hudson, J.A., Stephansson, O. & Anderson, J. 2005. Guidance on numerical modeling of thermo-hydro-mechanical coupled processes for performance assessment of radioactive waste repositories. *Int J of Rock Mech Min Sci.* 42: 850–870.

Kranz, R.L. 1983. Microcracks in rocks: A review. *Tectonophysics* 100:449–480.

Rutqvist, J., Barr, D., Datta, R., Gens, A., Millard, A., Olivella, S., Tsang, C-F. & Tsang, Y. 2005. Coupled thermal-hydrological-mechanical analysis of the Yucca Mountain Drift Scale Test- Comparison of field measurements to predictions of four different numerical models. *Int J of Rock Mech Min Sci.* 42: 680–697.

Zaman, M., Roegiers, J.-C., Abdulraheem, A. & Azeemuddin, M. 1994. Pore collapse in weakly cemented and porous rocks. *J of Energy Resources Tech* 116:97–103.